Supporting Information

Engineering porous Pd-Cu nanocrystals with tailored three-dimensional catalytic facets for highly efficient formic acid oxidation

Linfang Lu[a,*], Bing Wang[a], Di Wu[a], Shihui Zou[b,*] and Baizeng Fang[c,*]

[a] *College of Material, Chemistry and Chemical Engineering, Hangzhou Normal University, Hangzhou 311121, China. E-mail: linfang.lu@hznu.edu.cn*

[b] *Key Lab of Applied Chemistry of Zhejiang Province, Department of Chemistry, Zhejiang University, Hangzhou 310027, China. E-mail: xueshan199@163.com*

[c] *Department of Chemical and Biological Engineering, University of British Columbia, 2360 East Mall, Vancouver, BC V6T 1Z3, Canada. E-mail: bfang@chbe.ubc.ca*

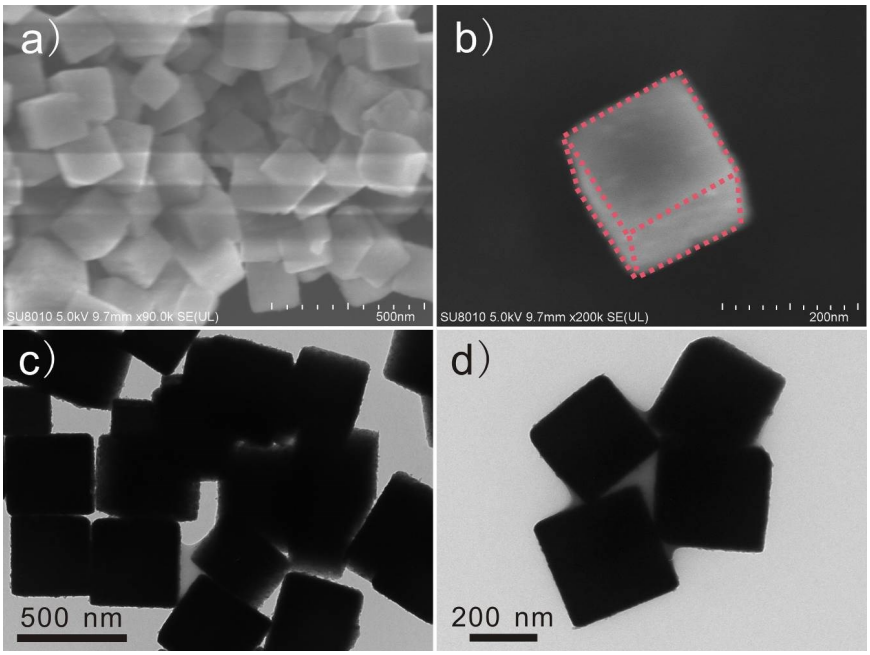

Figure S1. SEM images (a, b) and TEM images (c, d) with various magnifications of the as-synthesized cubic Cu_2O nanoparticles.

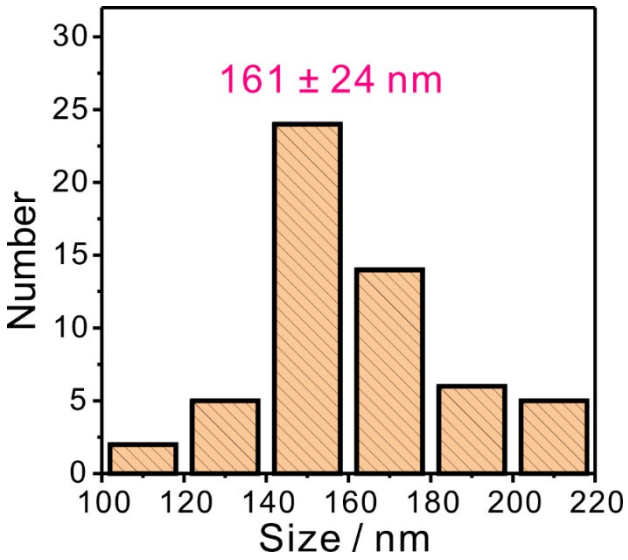

Figure S2. Particle size histogram for the original Cu_2O cubes.

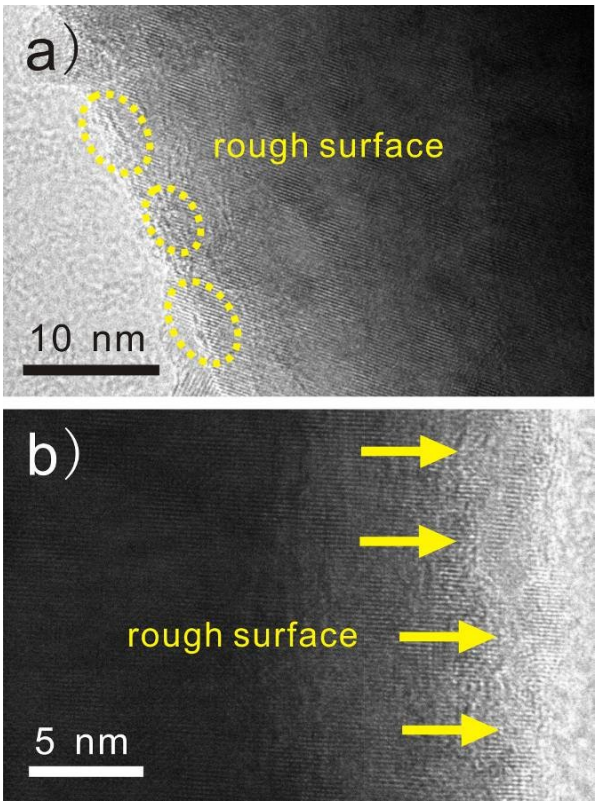

Figure S3. Surface morphology of the as-prepared cubic Cu_2O nanocrystals.

Table S1. The molar ratio of Pd to Cu of different Pd-Cu samples determined by STEM-EDX.

Samples	Pd/Cu
$Pd_{1/12}Cu$	1/69.3
$Pd_{1/6}Cu$	1/17.2
$Pd_{1/3}Cu$	1/10.5
Pd_1Cu	1/5.4
Pd_3Cu	1.8

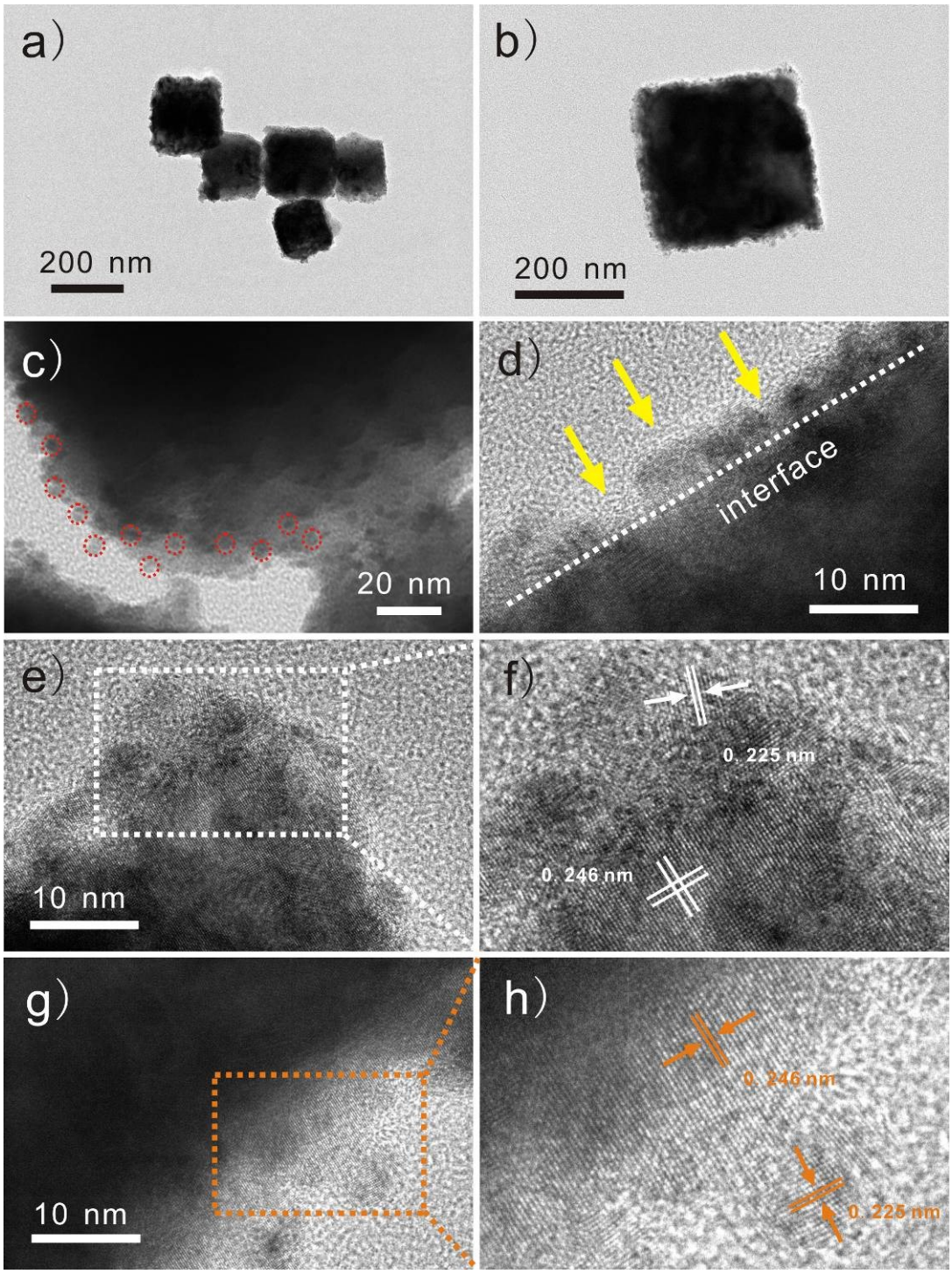

Figure S4. TEM (a-d) and HRTEM (e-h) images of $Pd_{1/12}Cu$.

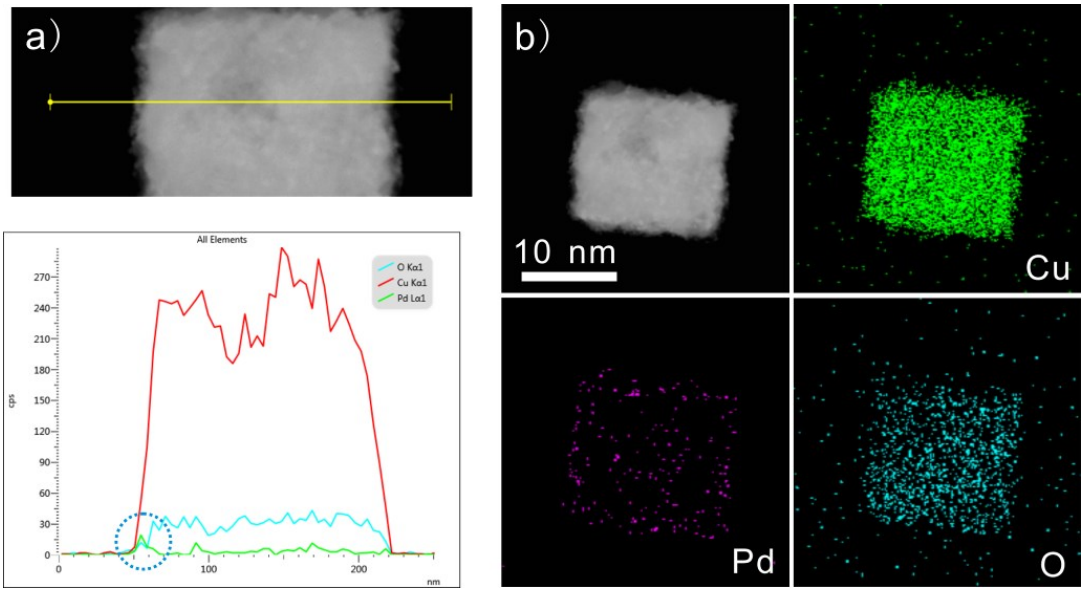

Figure S5. Line scan (a) and EDX mapping (b) of $Pd_{1/12}Cu$.

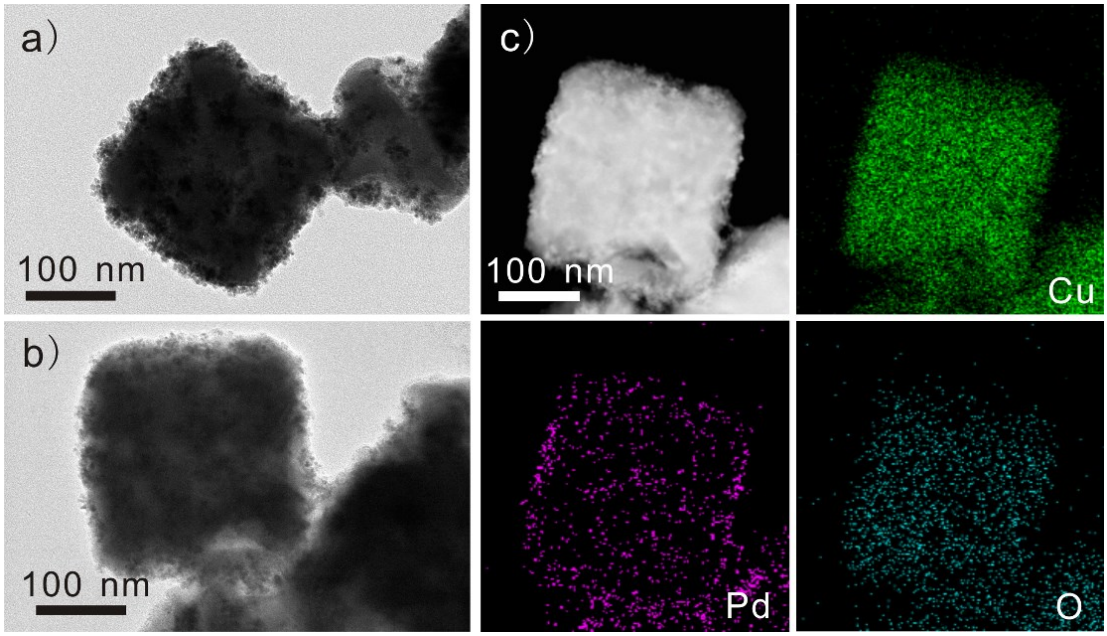

Figure S6. TEM images (a, b) and EDX mapping (c) of $Pd_{1/4.5}Cu$.

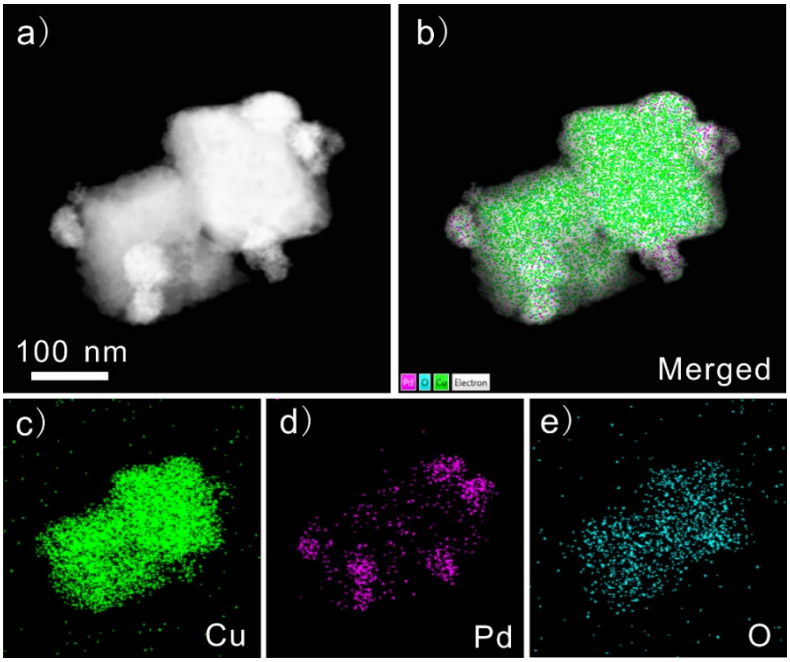

Figure S7. EDX mapping of PdCu nanoflower of $Pd_{1/3}Cu$.

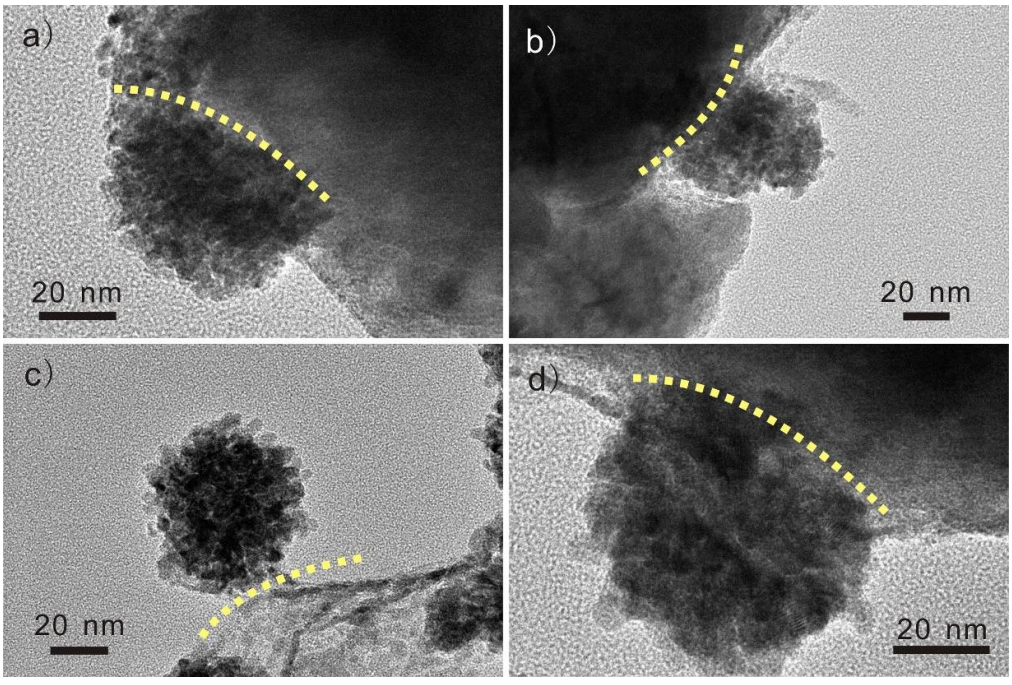

Figure S8. TEM images of $Pd_{1/3}Cu$, which show the formation of PdCu nanoflowers.

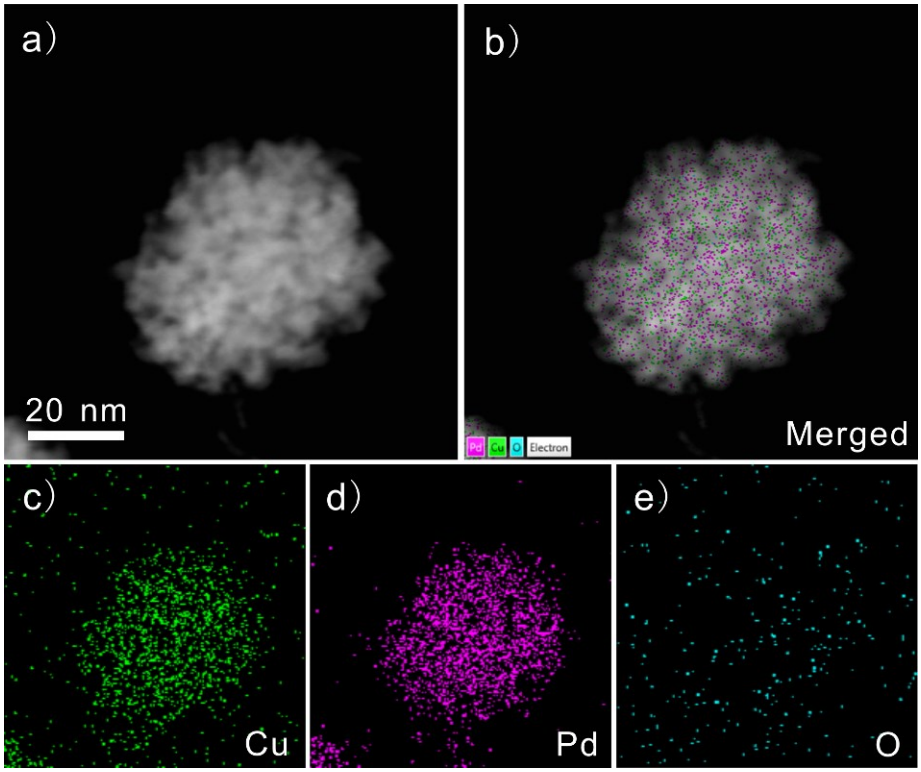

Figure S9. EDX mapping of PdCu nanoflower of $Pd_{1/3}Cu$.

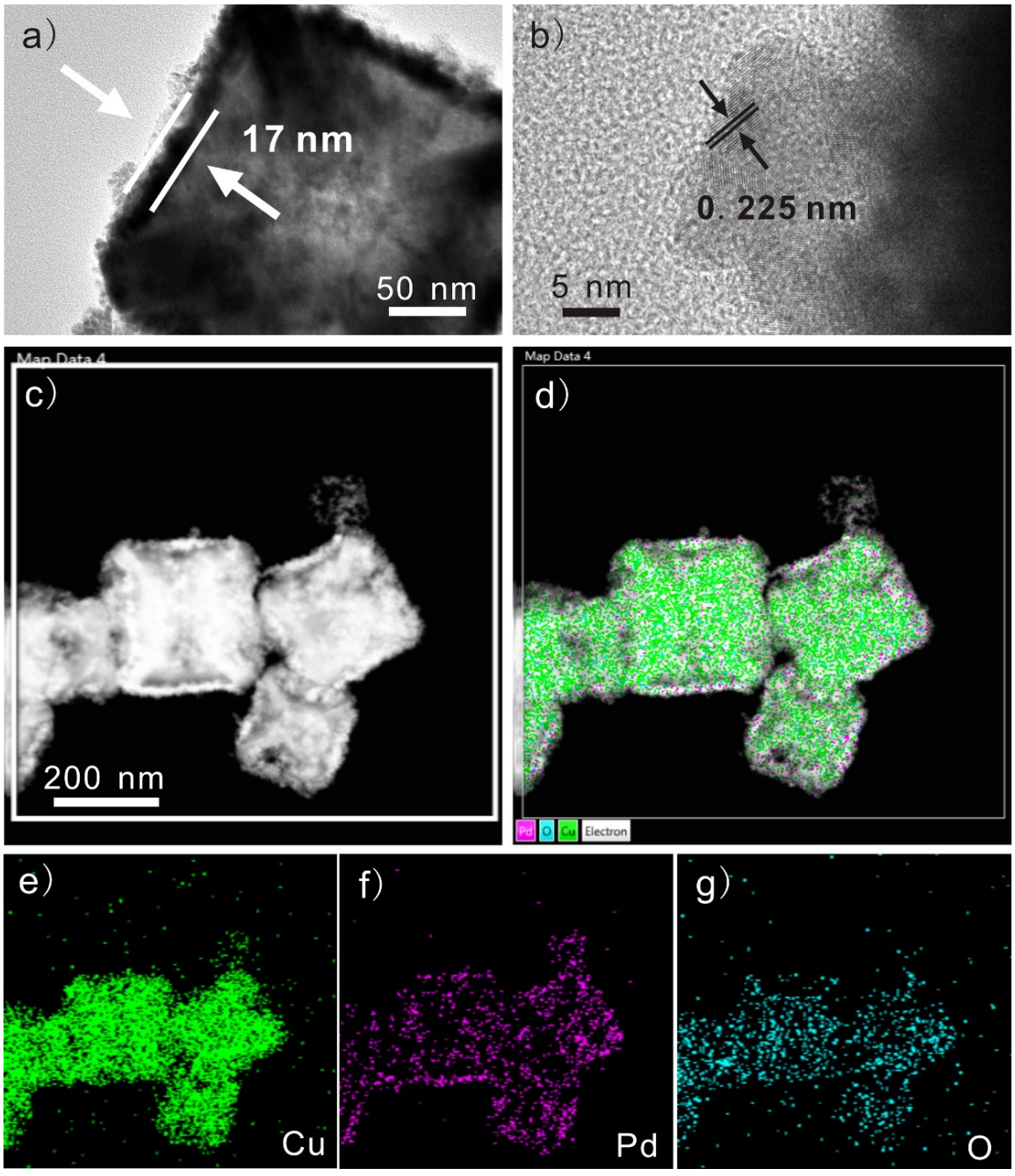

Figure S10. HRTEM images (a, b) and EDX mapping (c-g) of Pd_1Cu.

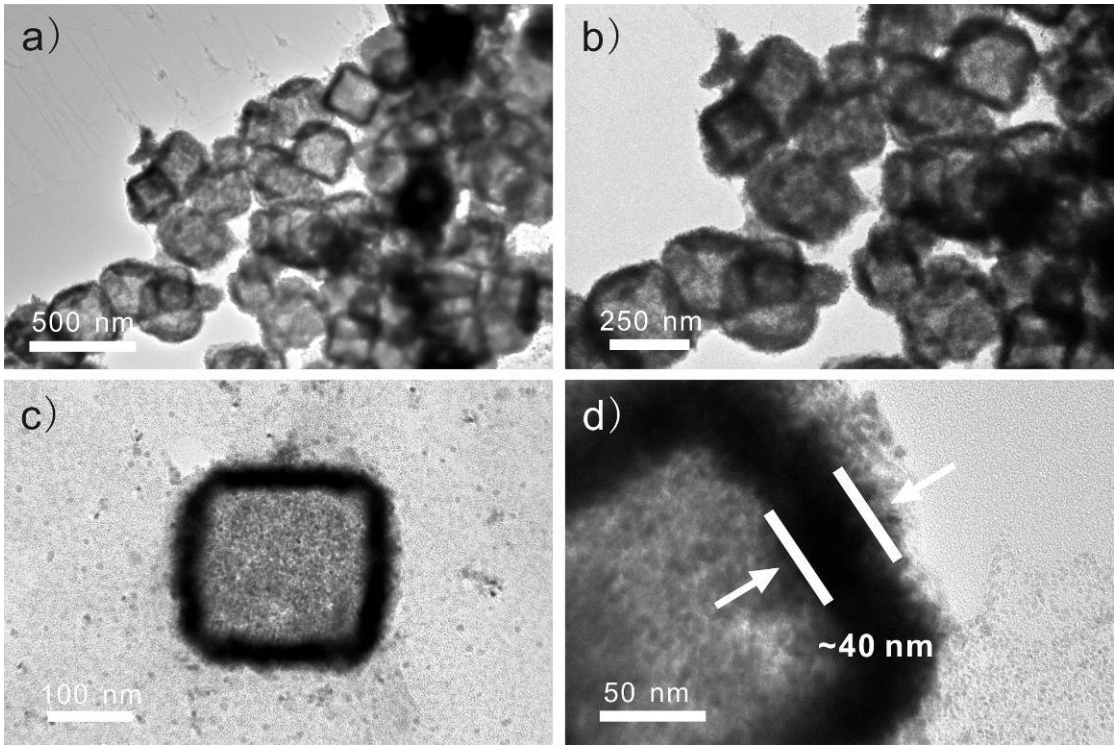

Figure S11. TEM images of Pd_3Cu.

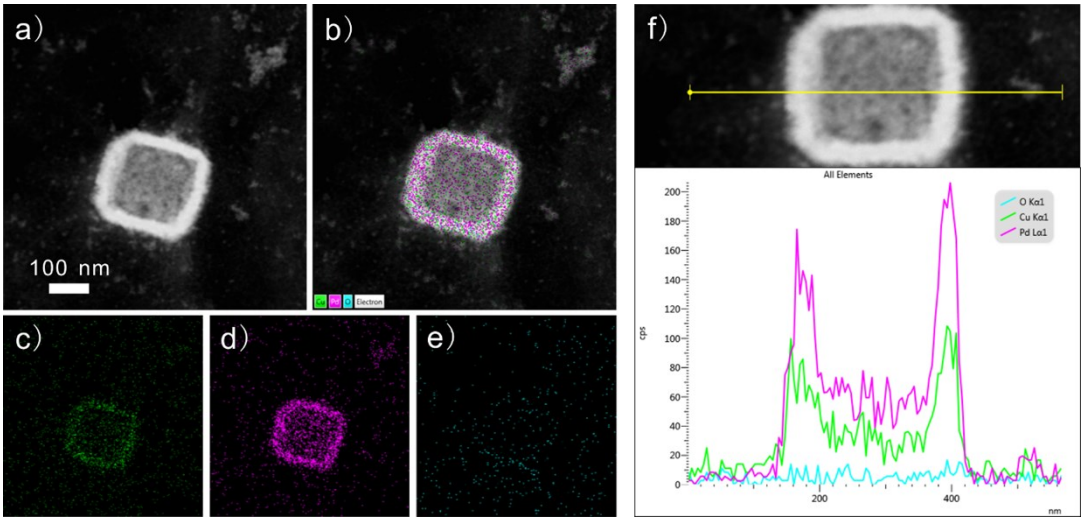

Figure S12. EDX mapping (a-e) and line scan (f) of Pd_3Cu.

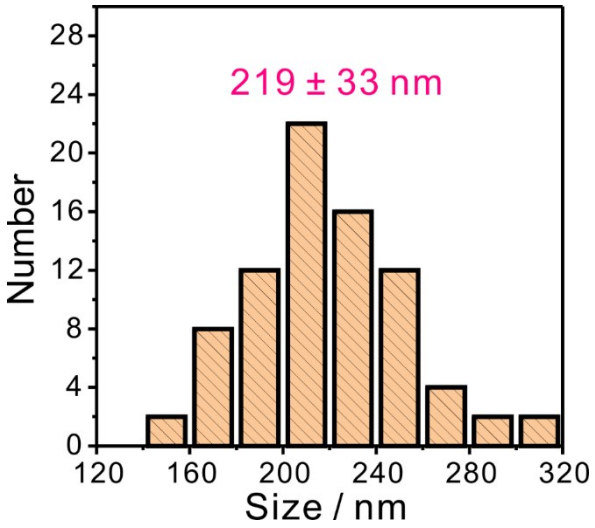

Figure S13. Particle size histogram for Pd_3Cu.

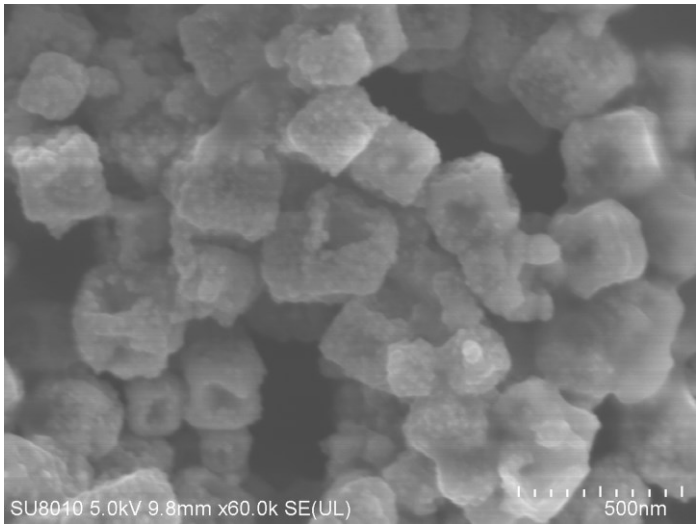

Figure S14. SEM image of Pd-Cu nanostructure with the molar ratio of 5:1 (Pd/Cu) of Pd and Cu precursors.

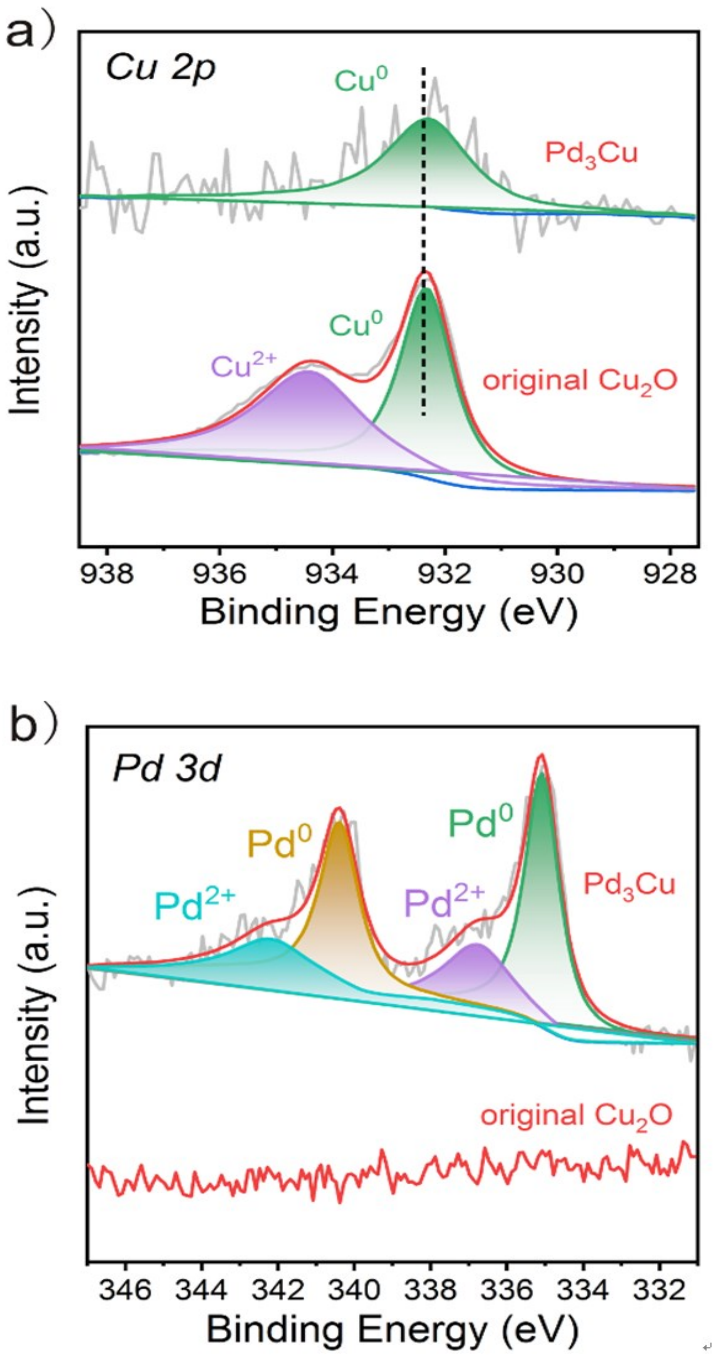

Figure S15. XPS spectra of Cu 2p (a) and Pd 3d (b) of the original Cu_2O and Pd_3Cu.

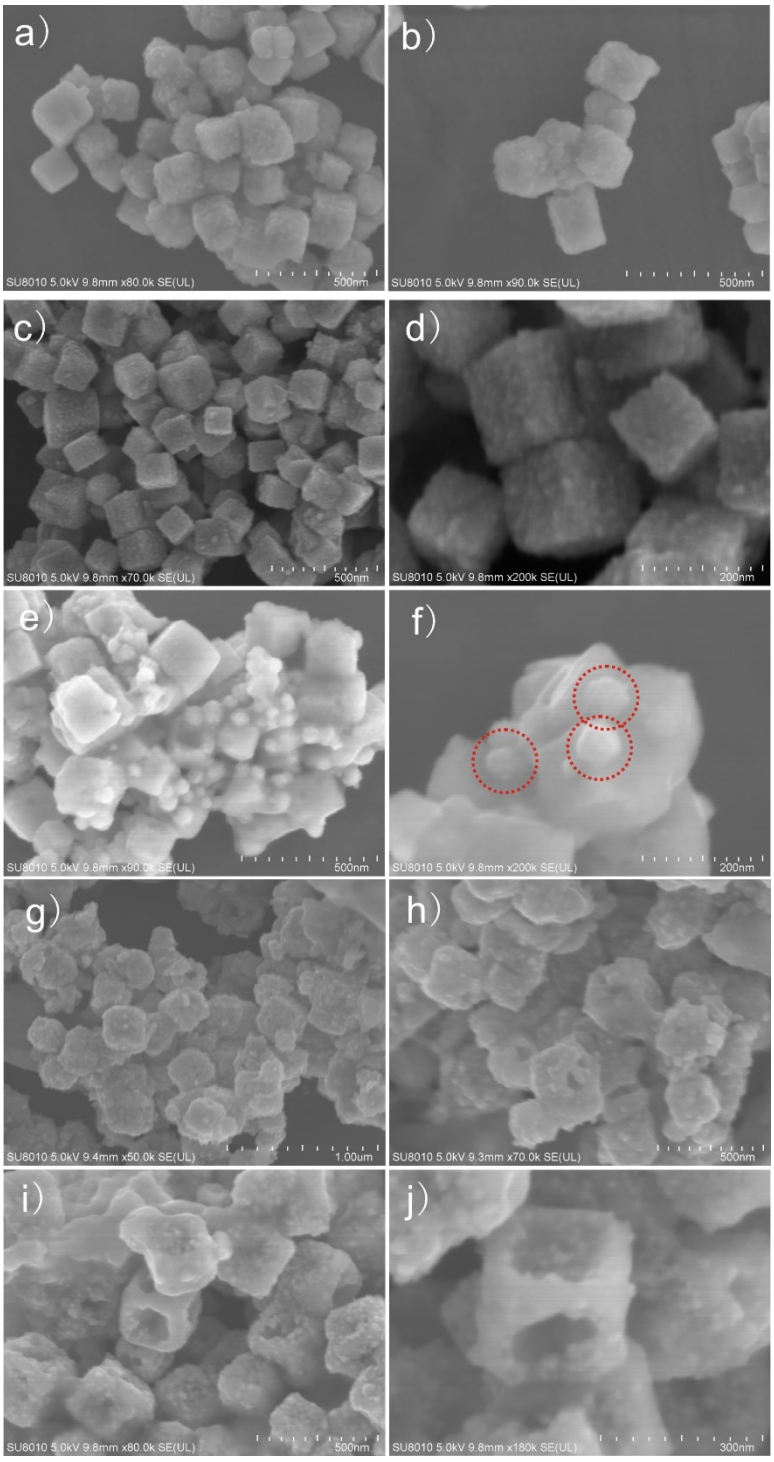

Figure S16. SEM images of the produced Pd-Cu nanostructure when the added mole ratio of Pd/Cu is 1/9 (a, b), 1/6 (c, d), 1/3 (e, f), 1 (g, h), 3 (i, j).

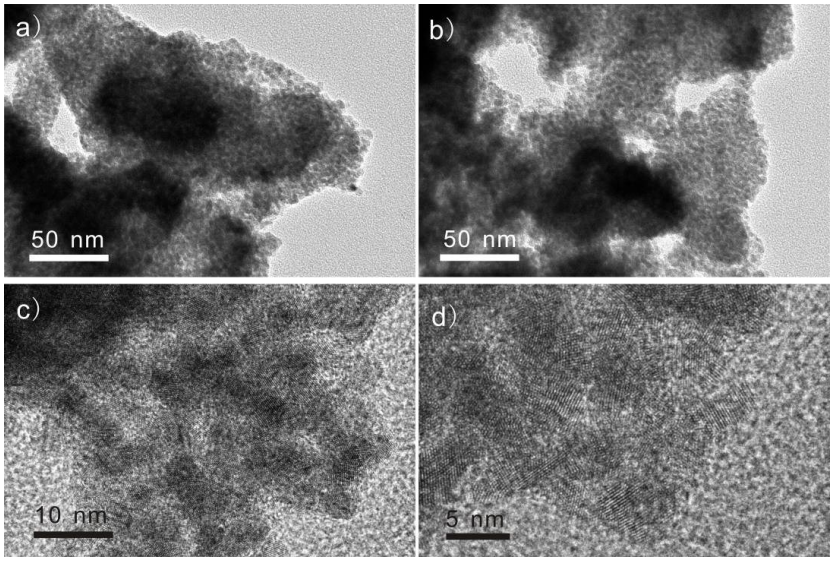

Figure 17. TEM (a,b) and HRTEM (c,d) images of the as-produced Pd-Cu nanostructure after the acid treatment when the molar ratio of the added Pd/Cu was 1/6. The sample is defined as PdCu AG-1.

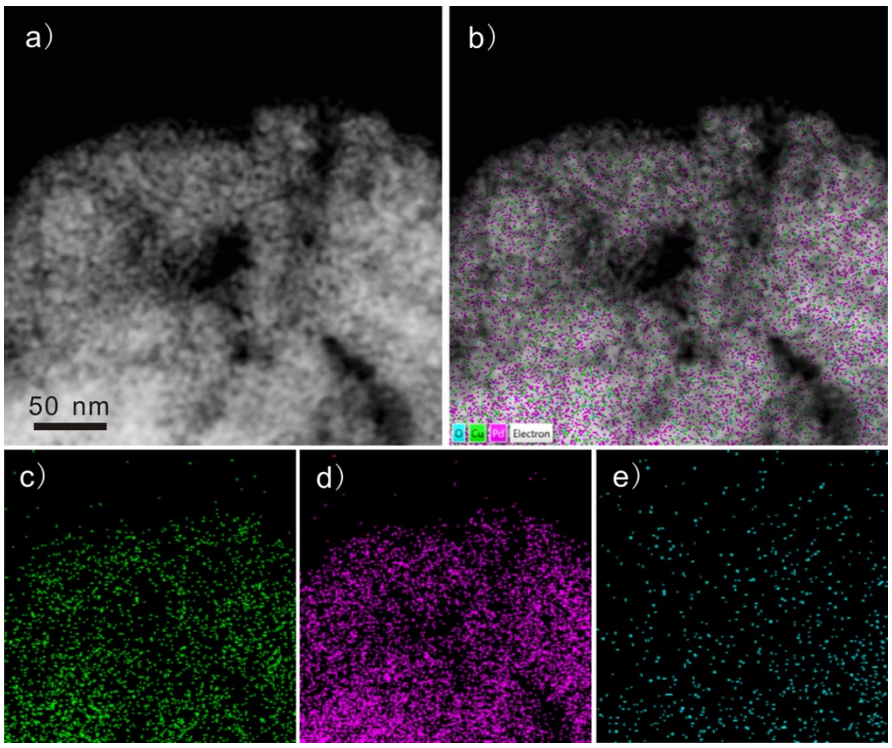

Figure 18. EDX mapping of PdCu AG-1

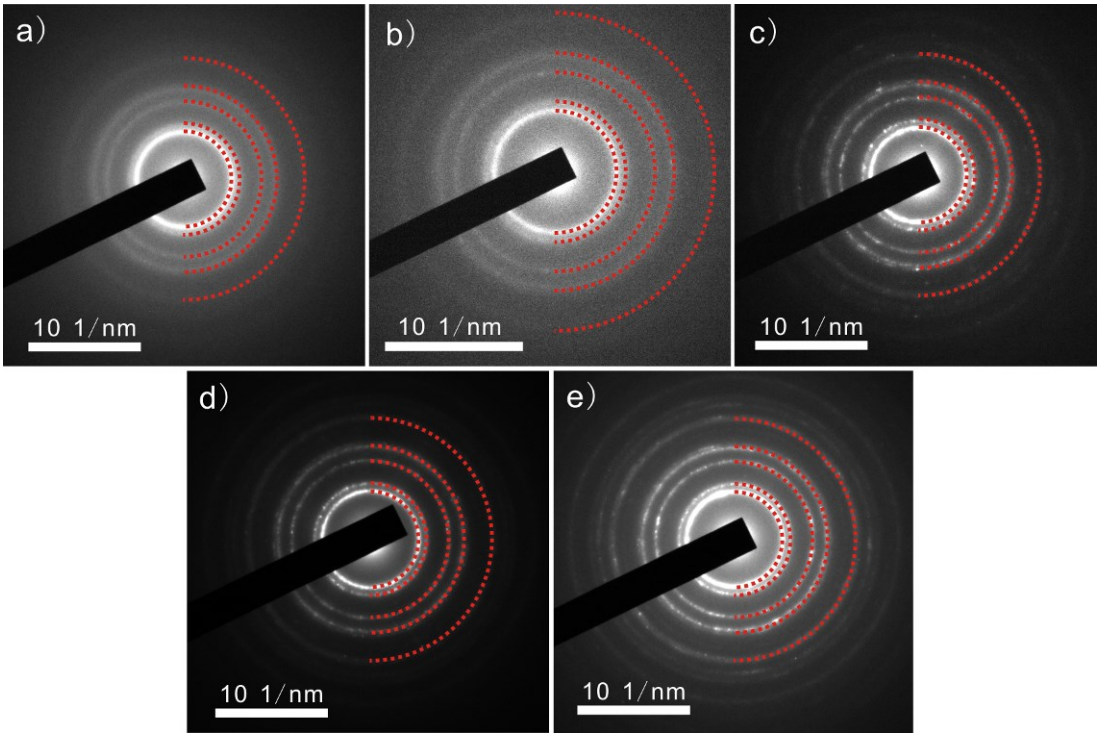

Figure 19. Selected area electron diffraction (SAED) of the as-produced Pd-Cu nanostructure after the acid treatment when the molar ratio of the added Pd/Cu was 1/9 (a), 1/6 (b), 1/3 (c), 1 (d), 3 (e), which corresponds to PdCu AG-1, PdCu AG-2, PdCu PND, PdCu MNC, PdCu PNB, respectively. The clear diffraction patterns indicate the formation of PdCu alloys after the acid treatment.

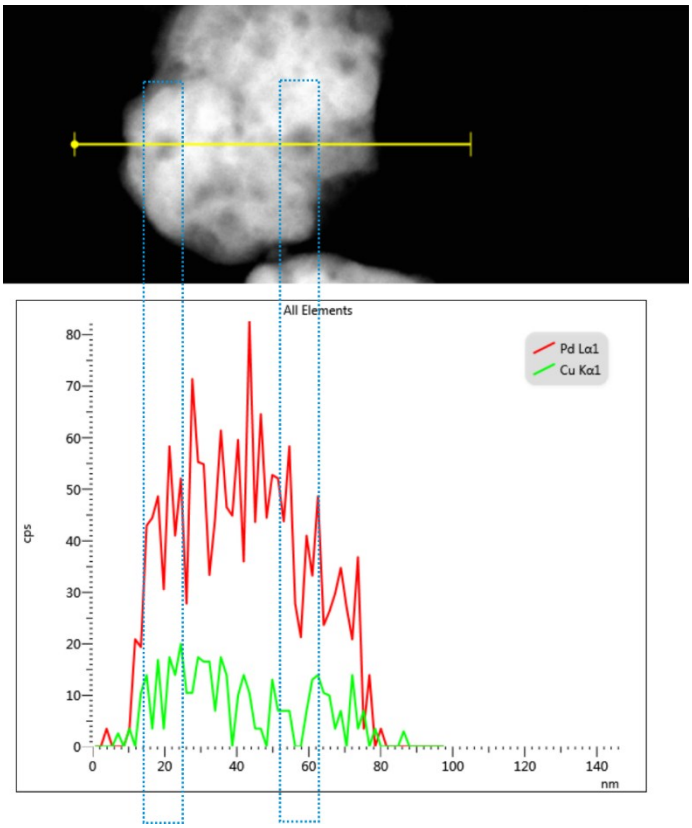

Figure 20. Line scan of a single particle of PdCu PND.

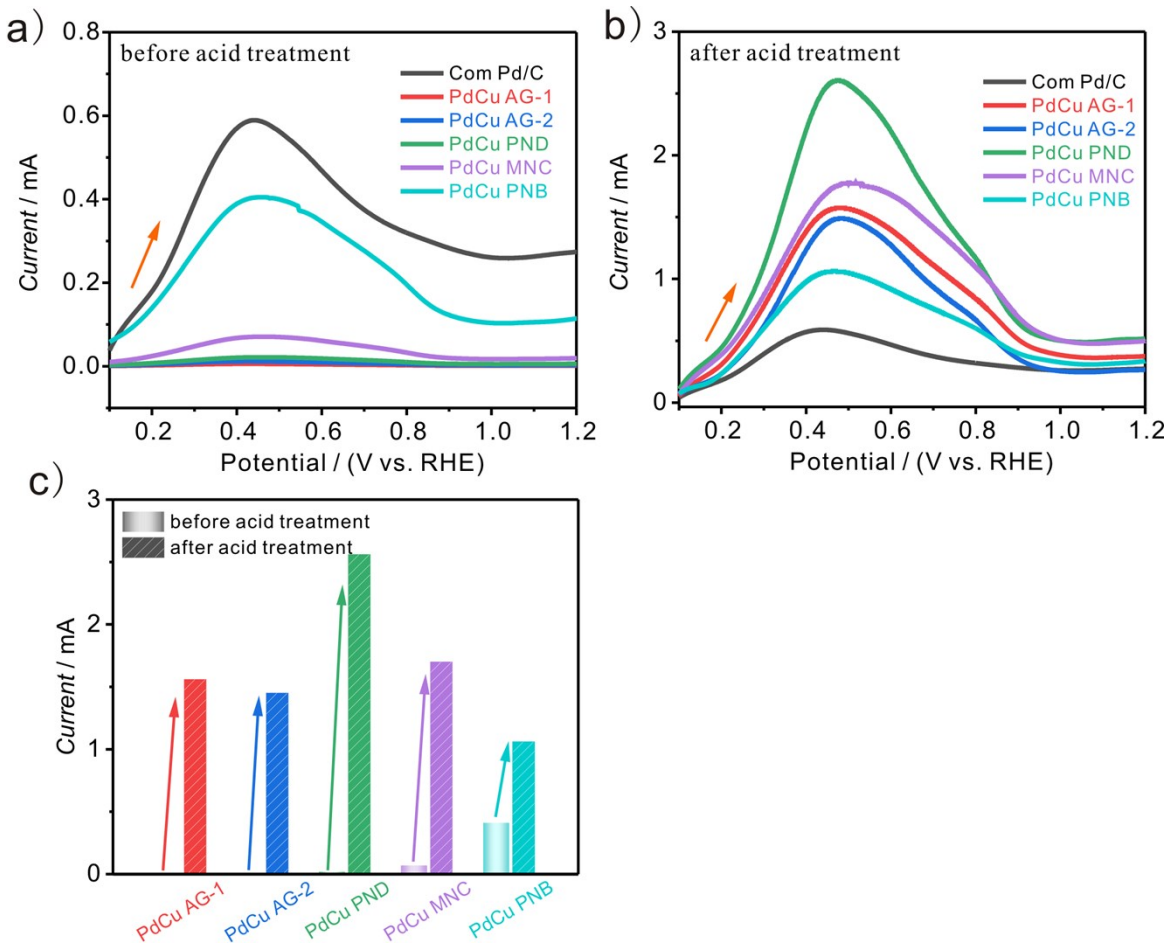

Figure S21. (a) FAO of the PdCu catalysts before acid treatment in 0.5 M H_2SO_4 + 0.5 M HCOOH. (b) FAO of the PdCu catalysts after acid treatment in 0.5 M H_2SO_4 + 0.5 M HCOOH. (c) The comparison of FOA activities of PdCu catalysts before and after acid treatment.

The currents of PdCu AG-1, PdCu AG-2, PdCu PND before acid treatment are very small (near 0 mA). This is because the relative content of Pd in the catalysts before acid treatment is too small. As shown in Table S1, the molar ratio of Pd to Cu of $Pd_{1/12}Cu$ sample is 1/69.3, while the molar ratio of Pd to Cu of $Pd_{1/6}Cu$ sample is 1/17.2, and the molar ratio of Pd to Cu of $Pd_{1/3}Cu$ sample is 1/10.5. It is difficult to maintain the same Pd content on the electrode. Therefore, we controlled the total mass of PdCu to be consistent. Although it is unfair to compare the activity before and after the acid treatment, the activity enhancement of PdCu PND sample shows that acid treatment can indeed increase the catalytic activity, whose Pd content is nearly consistent before and after the acid treatment.

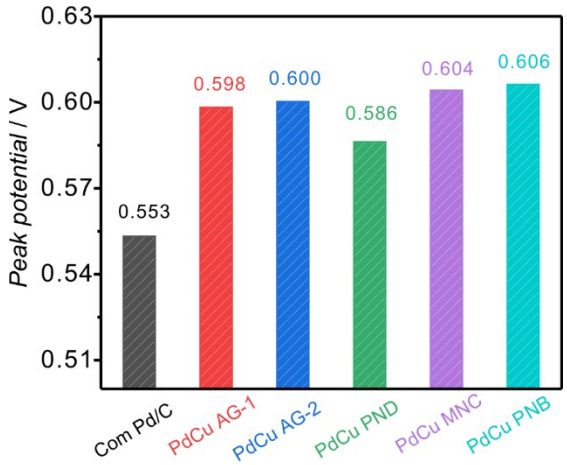

Figure S22. Peak potentials of PdO reduction of the different Pd-based samples from CVs in Figure 7a.

Table S2. *Summary of the activities of Pd-based catalysts for electrocatalytic FAO.*

Catalysts	Peak current densities (A mg^{-1})	Testing conditions	References
PdCu PND	2.46	0.5 M H_2SO_4 + 0.5 M HCOOH, 50 mV/s	This work
Pd nanosheets	0.63	0.1 M $HClO_4$ + 0.2 HCOOH, 50 mV/s	S1
Pd–Ni_2P	1.40	0.5 M H_2SO_4 + 0.5 M HCOOH, 50 mV/s	S2
3D PdCu alloyed nanostructure	1.84	0.5 M $HClO_4$ + 0.5 M HCOOH, 50 mV/s	S3
Pd–Ni–P	1.46	0.5 M H_2SO_4 + 0.5 M HCOOH, 50 mV/s	S4
Pd-NCs /rGO/MWCNTs	1.44	0.1 M $HClO_4$ + 1 M HCOOH, 50 mV/s	S5
$Pd_{0.6}/WO_{2.72}$	1.62	0.1 M $HClO_4$ + 0.1 M HCOOH, 50 mV/s	S6
Concave Pd nanocubes	0.33	0.1 M $HClO_4$ + 0.5 M HCOOH, 50 mV/s	S7
Pd nanosheets	1.38	0.5 M H_2SO_4 + 0.25 M HCOOH, 50 mV/s	S8
PdNiCu/C	0.79	0.5 M H_2SO_4 + 0.5 M HCOOH, 20 mV/s	S9
Pd/Graphene	0.09	0.5 M H_2SO_4 + 0.5 M HCOOH, 50 mV/s	S10
PdAg	0.52	0.1 M $HClO_4$+ 0.1 M HCOOH, 50 mV/s	S11
Pd_3Fe	0.70	0.5 M H_2SO_4 + 0.5 M HCOOH, 50 mV/s	S12
Pd-Fe_2P/C	1.45	0.5 M H_2SO_4 + 0.5 M HCOOH, 50 mV/s	S13
PdO/Pd-CeO_2	1.62	0.5 M H_2SO_4 + 0.5 M HCOOH, 50 mV/s	S14
CuPd@Pd tetrahedra	0.50	0.5 M H_2SO_4 + 0.5 M HCOOH, 50 mV/s	S15

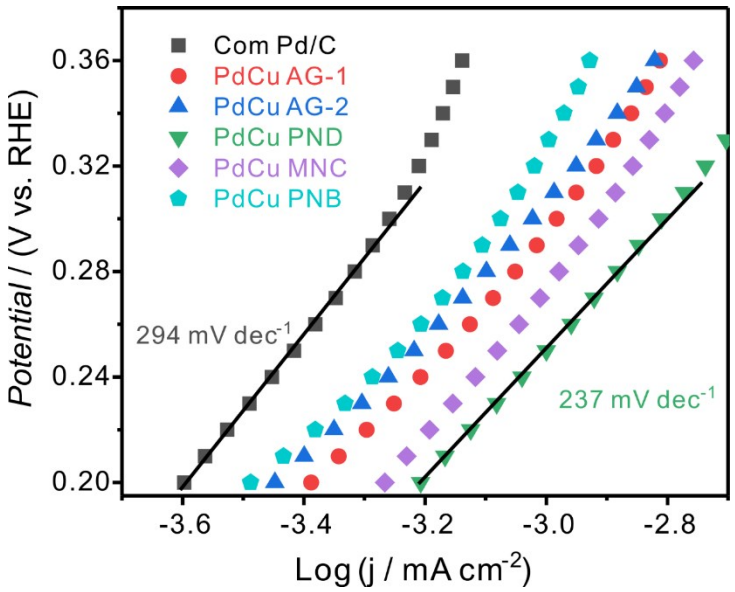

Figure S23. Tafel plots for the commercial Pd/C and PdCu AG-1, PdCu AG-2, PdCu PND, PdCu MNC, PdCu PNB catalysts.

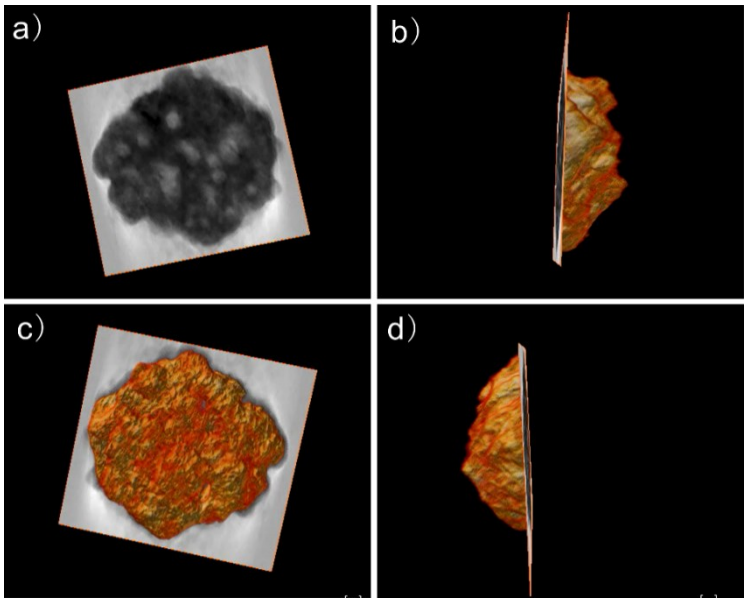

Figure S24. 3D reconstruction of hemispheroid of a single PdCu porous nanodendrite (PND) particle.

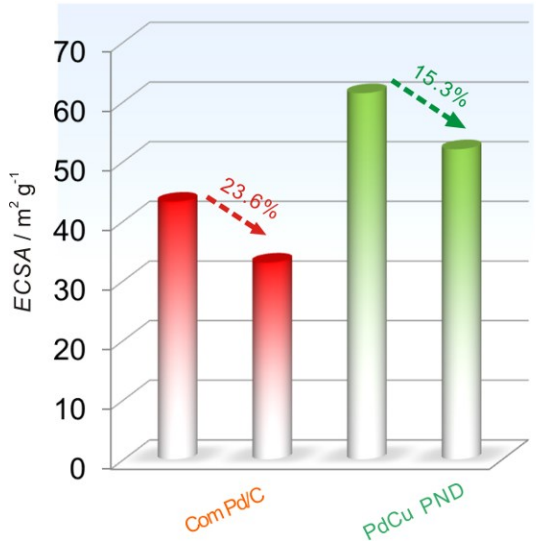

Figure S25. The variation of the ECSAs of the commercial Pd/C and PdCu PND before and after the stability test.

References

S1. Zhang, Y.; Wang, M.; Zhu, E.; Zheng, Y.; Huang, Y.; Huang, X. Seedless growth of palladium nanocrystals with tunable structures: from tetrahedra to nanosheets. *Nano Lett.* **2015**, 15, 7519-7525.

S2. Chang, J.; Feng, L.; Liu, C.; Xing, W.; Hu, X. An effective Pd–Ni_2P/C anode catalyst for direct formic acid fuel cells. *Angew. Chem. Int. Ed.* **2014**, 53, 122-126.

S3. Jiang, B.; Li, C.; Malgras, V.; Bando, Y.; Yamauchi, Y. Three-dimensional hyperbranched PdCu nanostructures with high electrocatalytic activity. *Chem. Commun.* **2016**, 52, 1186-1189.

S4. Liang, X.; Liu, B.; Zhang, J.; Lu, S.; Zhuang, Z. Ternary Pd–Ni–P hybrid electrocatalysts derived from Pd–Ni core–shell nanoparticles with enhanced formic acid oxidation activity. *Chem. Commun.* **2016**, 52, 11143-11146.

S5. Yousaf, A. B.; Imran, M.; Zeb, A.; Xie, X.; Liang, K.; Zhou, X.; Yuan, C. Z.; Xu, A. W. Synergistic effect of graphene and multi-walled carbon nanotubes composite supported Pd nanocubes on enhancing catalytic activity for electro-oxidation of formic acid. *Catal. Sci. Technol*. **2016**, 6, 4794-4801.

S6. Xi, Z.; Erdosy, D. P.; Mendoza-Garcia, A.; Duchesne, P. N.; Li, J.; Muzzio, M.; Li, Q.; Zhang, P.; Sun, S. Pd nanoparticles coupled to $WO_{2.72}$ nanorods for enhanced electrochemical oxidation of formic acid. *Nano Lett.* **2017**, 17, 2727-2731.

S7. Vara, M.; Lu, P.; Yang, X.; Lee, C. T.; Xia, Y. A photochemical, room-temperature, and aqueous route to the synthesis of Pd nanocubes enriched with atomic steps and terraces on the side faces. *Chem. Mater.* **2017**, 29, 4563-4571.

S8. Huang, X.; Tang, S.; Mu, X.; Dai, Y.; Chen, G.; Zhou, Z.; Ruan, F.; Yang, Z.; Zheng, N. Freestanding palladium nanosheets with plasmonic and catalytic properties. *Nat. Nanotech.* **2011**, 6, 28.

S9. Hu, S.; Munoz, F.; Noborikawa, J.; Haan, J.; Scudiero, L.; Ha, S. Carbon supported Pd-based bimetallic and trimetallic catalyst for formic acid electrochemical oxidation. *Appl. Catal. B-Environ.* **2016**, 180, 758-765.

S10. Zhang, L. Y.; Zhao, Z. L.; Li, C. M. Formic acid-reduced ultrasmall Pd nanocrystals on graphene to provide superior electocatalytic activity and stability toward formic acid oxidation. *Nano Energy* **2015**, 11, 71-77.

S11. Liu, D.; Xie, M.; Wang, C.; Liao, L.; Qiu, L.; Ma, J.; Huang, H.; Long, R.; Jiang J.; Xiong, Y. Pd-Ag alloy hollow nanostructures with interatomic charge polarization for enhanced electrocatalytic formic acid oxidation. *Nano Res.* **2016**, 9, 1590-1599.

S12. Liu, Z.; Fu, G.; Li, J.; Liu, Z.; Xu, L.; Sun, D.; Tang, Y. Facile synthesis based on novel carbon-supported cyanogel of structurally ordered Pd_3Fe/C as electrocatalyst for formic acid oxidation. *Nano Res.* **2018**, 11, 4686-4696.

S13. Wang, F.; Xue, H.; Tian, Z.; Xing, W.; Feng, L. Fe_2P as a novel efficient catalyst promoter in Pd/C system for formic acid electro-oxidation in fuel cells reaction. *J. Power Sources* **2018**, 375, 37-42.

S14. Zhang, L.; Ding, L. X.; Luo, Y.; Zeng, Y.; Wang, S.; Wang, H. PdO/Pd-CeO_2 hollow spheres with fresh Pd surface for enhancing formic acid oxidation. *Chem. Eng. J.* **2018**, 347, 193-201.

S15. Chen, Y.; Yang, Y.; Fu, G.; Xu, L.; Sun, D.; Lee, J. M.; Tang, Y. Core–shell CuPd@Pd tetrahedra with concave structures and Pd-enriched surface boost formic acid oxidation. *J. Mater. Chem. A* **2018**, 6, 10632-10638.